Crowding Effects of Membrane Proteins

ARTICLE *in* THE JOURNAL OF PHYSICAL CHEMISTRY B · APRIL 2009

Impact Factor: 3.3 · DOI: 10.1021/jp8107446 · Source: PubMed

1 AUTHOR:

Huan-Xiang Zhou
Florida State University
259 PUBLICATIONS **10,211** CITATIONS

SEE PROFILE

FEATURE ARTICLE

Crowding Effects of Membrane Proteins

Huan-Xiang Zhou†

Department of Physics and Institute of Molecular Biophysics, Florida State University, Tallahassee, Florida 32306

Received: December 6, 2008; Revised Manuscript Received: January 29, 2009

In cell membranes, membrane proteins occupy ~30% of the total surface area. Crowding effects similar to those in the solution phase are thus to be expected. In addition, there are crowding effects unique to proteins bound to the two-dimensional membranes, such as those exerted on the equilibration of a protein between two membrane orientations and on the redistribution of proteins between different locations in a cell membrane. This article aims to present a theoretical framework for understanding the various crowding effects within membranes. For illustration, the theory is used to analyze previously published experimental and simulation data. It is hoped that the article will encourage quantitative analyses in future experiments and spur systematic investigation of membrane crowding effects.

Introduction

In the past few years, effects of macromolecular crowding in solutions and in the cytosol have attracted great attention. Theories predict significant influences by macromolecular crowding on the thermodynamics and kinetics of protein folding, binding, and aggregation;[1,2] in many cases, these predictions are borne out by experimental observations (for a recent review, see ref 3). In cell membranes, the area fraction occupied by proteins ranges from 15 to 35%,[4,5] which is comparable to the volume fraction occupied by macromolecules in the cytosol.[6] Therefore, we expect similar influences by crowding of membrane proteins on their folding, binding, and aggregation. Theoretical predictions about crowding effects of membrane proteins have been made,[7−11] Monte Carlo simulations have been used to model the binding equilibria and kinetics of membrane proteins under crowding,[12,13] and a few experimental studies have been designed specifically to investigate crowding of membrane proteins.[11,14−16] The aim of this article is to present a theoretical framework for analyzing the various crowding effects within membranes. It is hoped that the illustrative results presented here will spur greater attention to membrane crowding, especially by experimentalists.

By membrane crowding, we refer to the presence of proteins in high densities in a membrane, such that thermodynamic and kinetic properties of processes involving one or a few protein molecules are altered. A process involving a single protein molecule is the partitioning between two membrane orientations or between the membrane and solution phases (Figure 1a,b). A process involving two protein molecules is dimerization (Figure 1c). Much like the situation in the solution phase, a universal aspect of crowding among all of the protein molecules in a membrane is the mutual exclusion of their solid volumes. This volume exclusion, which by itself increases the chemical potential of each species of membrane protein, is the focus of this article.

† Phone: (850) 645-1336. Fax: (850) 644-7244. E-mail: hzhou4@fsu.edu.

We pay special attention to the localization of membrane proteins to a two-dimensional space. In particular, the translational freedom of membrane proteins along the membrane normal is greatly limited in comparison to that within the membrane plane. Similarly, the rotation around an axis within the membrane plane is severely restricted in comparison to that around the membrane normal, such that the proteins appear to have defined orientations relative to the membrane plane. Therefore, for the purpose of accounting for volume exclusion, a membrane protein can be effectively treated as a two-dimensional object, as represented by the cross section within the membrane plane.[17] The level of crowding is then measured by the total area fraction of all of the membrane proteins, in analogy to the volume fraction in the solution phase.

The restriction to a two-dimensional membrane gives rise to distinct features to membrane proteins with regard to crowding. The reduction in dimensionality, from three to two, of the membrane phase means that a similar level of crowding is achieved with far fewer protein molecules than needed in the solution phase. This fact has two important consequences. First, it means that variations in copy numbers of membrane proteins, either through the life cycle of a cell or among different parts of the same membrane, for example, in microdomains such as lipid rafts,[18,19] can have a significant influence on crowding effects. Second, unlike the situation in the cytosol, where a large number of different species of macromolecules are present, each by itself not necessarily at a high concentration, the number of different species of membrane proteins is relatively small, but the surface densities of the individual species can be relatively high. Therefore, self-crowding, exerted by other molecules of the same species, can be important in the membrane phase.

Another distinct feature of membrane proteins arises from the fact, noted above, that they have defined orientations relative to the membrane plane. For some proteins, more than one orientation can be adopted (Figure 1a). Because different membrane orientations have different cross sections and the effects of membrane crowding depend on the cross sections, one can expect that crowding affects the partitioning of a membrane among its possible membrane orientations.

10.1021/jp8107446 CCC: $40.75
Published on Web 03/26/2009

Huan-Xiang Zhou received his Ph.D. from Drexel University in 1988. He did postdoctoral work at the NIH with Attila Szabo. After faculty appointments at HKUST and Drexel, he moved to Florida State University in 2002. His group does theoretical, computational, and experimental research on protein−protein interactions, on crowding and confinement effects of cellular environments, and on biological roles of protein dynamics. He is currently the Editor-in-Chief of PMC Biophysics.

Modeling of Crowding by Scaled Particle Theory

Within the membrane plane, area exclusion among the cross sections of all of the membrane proteins serves to increase the chemical potential of every species. The increase in chemical potential comes about because some of the positions and orientations of each protein molecule are eliminated due to overlap with other protein molecules. Suppose that the density, that is, the number of molecules per unit area of the membrane plane, of species α is c_α. The chemical potential of species α can be written as the sum of an ideal part and the increase due to crowding

$$\mu_\alpha = k_B T \ln(c_\alpha/\Lambda_\alpha) + \Delta\mu_\alpha \quad (1)$$

where k_B is Boltzmann's constant, T is the absolute temperature, and Λ_α is a constant determined by the intrinsic properties of a species α molecule. Note that $-k_B T \ln\Lambda_\alpha$ is the two-dimensional equivalent of the standard chemical potential in a dilute solution.

The increase in chemical potential, $\Delta\mu_\alpha$, is equal to the work, W_α, required to place a single α molecule into the membrane plane while all of the membrane proteins are present in their respective densities. Let us now consider placing an arbitrary test molecule into such a distribution of membrane proteins, which we now refer to as crowders. The crowders preclude a fraction of the placements due to overlap (Figure 2a). The work, W, required to place the test molecule is related to the fraction, f, of successful placements, that is, those not incurring overlap with any crowder, by

$$W = -k_B T \ln f \quad (2)$$

The desired quantity, W_α, is obtained when the test molecule takes the cross section of species α.

For the special case of a point-like test molecule, the fraction of successful placements is simply the fraction of area not covered by the crowders. If the cross section of species α has area s_α, the fraction of area covered by the crowders is

$$\phi = \sum_\alpha s_\alpha c_\alpha \quad (3)$$

For the point-like test molecule, we have $f = 1 - \phi$. For a test molecule with a finite cross section, the region excluded by each crowder includes not only the cross section of the crowder but also a surrounding area (Figure 2b). Now, f is the fraction of area not covered by such "expanded" cross sections of the crowders (Figure 2c) or, equivalently

$$f = 1 - \phi_{exp} \quad (4)$$

where ϕ_{exp} is the fraction of area covered by the expanded cross

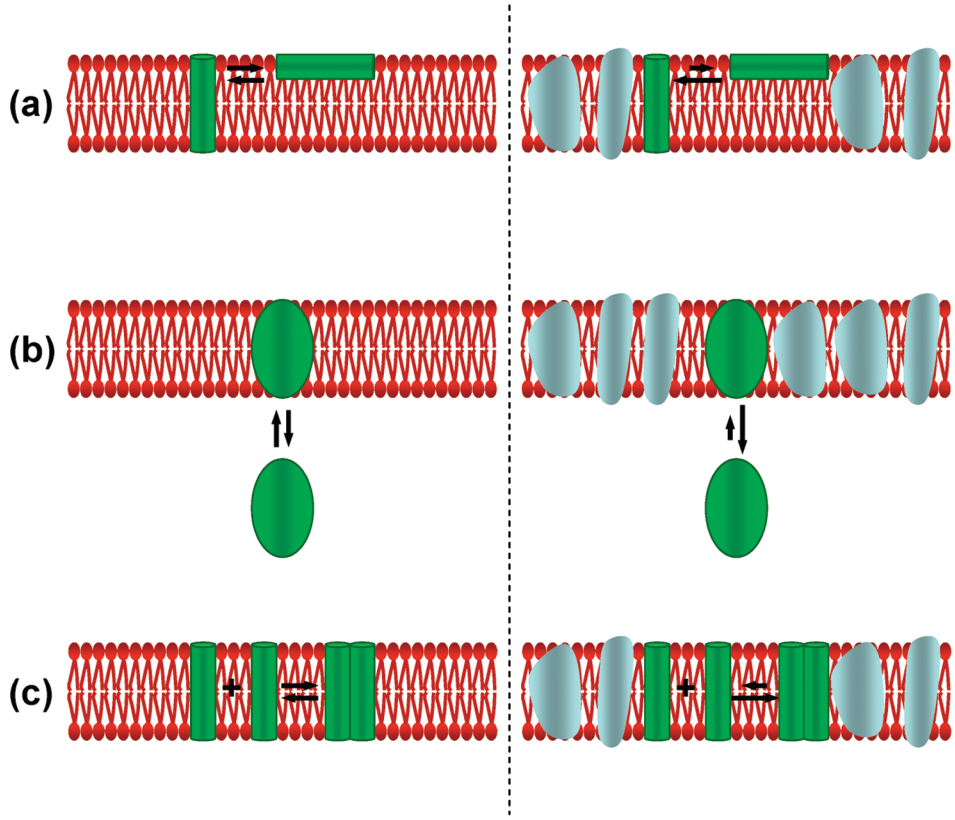

Figure 1. Illustration of membrane crowding. Depicted on the left and right of the vertical dashed line are processes occurring in the absence and presence of crowders, as represented by cyan objects inserted in the membrane. (a) Equilibration between two membrane orientations (a transmembrane helix, with a smaller cross section, becomes more favorable under crowding). (b) Equilibration between the membrane and solution phases. (c) Dimerization.

sections of the crowders. However, ϕ_{exp} is not simply given by eq 3 with an expanded area for each species of crowders. That is because the expanded cross sections, unlike the original ones, can overlap (Figure 2c). Therefore, the total covered area would be less than the sum of the areas of the expanded cross sections.

The scaled particle theory[20] builds in part on the above idea of expanded cross sections of the crowders. More precisely, it introduces a test molecule with a negative size, such that the effective cross sections of the crowders are shrunk instead of expanded. Then, there is no problem of overlapping cross sections, and ϕ_{exp} can be calculated by eq 3 with a shrunk area for each species of crowders. When each species of crowders has a circular cross section with radius R_α, and the test molecule has a radius $R \leq 0$, we have

$$W = -k_B T \ln\left[1 - \sum_\alpha 4\pi(R_\alpha + R)^2 c_\alpha\right] \qquad R \leq 0 \quad (5)$$

In the end, only the values of W and its first derivative with respect to R, calculated at $R = 0$, are used for completing the theory. A second piece of the scaled particle theory is a three-term expansion of W in terms of the size of the test molecule

$$W = W_0 + W_1 l + W_2 s \quad (6)$$

where W_0, W_1, and W_2 are expansion coefficients; $l = 2\pi R$ is the circumference of the test particle, and $s = \pi R^2$ is the area. Such an expansion is valid in the $R \to \infty$ limit but is assumed to be valid for any R. The first two expansion coefficients are determined by the aforementioned values of W, and its first derivative is determined at $R = 0$; the last coefficient, which can be interpreted as the pressure, P, can be obtained self-consistently by a thermodynamic relation between chemical potential and pressure, $(\partial P/\partial c_\alpha) = \sum_{\alpha'} c_{\alpha'}(\partial \mu_{\alpha'}/\partial c_\alpha)$, where the partial derivatives are taken while holding the temperature, volume, and the numbers of molecules of all species but α constant. The final result for $\Delta\mu_\alpha$ is

$$\frac{\Delta\mu_\alpha}{k_B T} = -\ln(1-\phi) + \frac{l_\alpha c_l/2\pi + s_\alpha c}{1-\phi} + \frac{s_\alpha c_l^2/4\pi}{(1-\phi)^2} \quad (7)$$

where l_α is the circumference of species α, and

$$c = \sum_\alpha c_\alpha \quad (8a)$$

$$c_l = \sum_\alpha l_\alpha c_\alpha \quad (8b)$$

The scaled particle theory has a long history of being used to analyze effects of macromolecular crowding in the solution phase;[21−25] its specialization to two dimensions, as just outlined, has also found use.[7−11,15,16] The final result, eq 7, is written in a form that is valid not just for crowders with circular cross sections but for particles with convex cross sections in general.[26] This equation is central to the analyses to be presented below.

Partitioning between Membrane Orientations

As noted above, a membrane protein has a defined orientation relative to the membrane plane. In some cases, a protein can adopt more than one distinct membrane orientation. The two-dimensional scaled particle theory has been used to analyze the equilibria between membrane orientations,[11,16] which are equivalent to those between conformations of a membrane protein.[9] Here, we illustrate the problem on a membrane-bound helical peptide, which may either adopt a transmembrane orientation or lie in the membrane−water interface, to be referred to as the in-plane orientation (Figure 1a). The two orientations have different cross sections. The different cross sections mean that the crowding effects experienced by the helical peptide in the two orientations are different. Therefore, crowding will affect the equilibration between these two orientations.

We now consider the populations in the two membrane orientations as two species, denoted as "tr" and "in", respectively. If the total density of the bound peptide is c, then

$$c = c_{tr} + c_{in} \quad (9)$$

At equilibrium, the chemical potential of the two species are equal

$$\mu_{tr} = \mu_{in} \quad (10)$$

These two conditions determine the densities of the two species.

In the dilute limit (i.e., $c \to 0$), only the ideal part of the chemical potential is important. Equation 10 then leads to

$$c_{tr}/\Lambda_{tr} = c_{in}/\Lambda_{in} \quad (11a)$$

or

$$\frac{c_{tr}}{c_{in}} = \frac{\Lambda_{tr}}{\Lambda_{in}} \equiv K_{o0} \quad (11b)$$

The last identity defines the equilibrium constant between the two membrane orientations in the dilute limit. Combining with eq 9, we find

$$c_{tr} = \frac{K_{o0}}{1 + K_{o0}} c \quad (12a)$$

$$c_{in} = \frac{1}{1 + K_{o0}} c \quad (12b)$$

as $c \to 0$.

At higher densities, crowding between peptide molecules comes into play. We can write eq 10 in the form

$$\frac{c_{tr}}{c_{in}} = \frac{\Lambda_{tr}}{\Lambda_{in}} e^{-(\Delta\mu_{tr} - \Delta\mu_{in})/k_B T} = K_{o0} e^{-(\Delta\mu_{tr} - \Delta\mu_{in})/k_B T} \quad (13)$$

Note that the increases in chemical potential, $\Delta\mu_\alpha$, α = tr and in, are functions of c_α (see eq 7). Equation 13 thus presents an implicit relation between c_{tr} and c_{in}. The values of c_{tr} and c_{in} can be determined by iteration (see the Appendix).

A complication is that the in-plane can be present in both leaflets of the membrane, but the peptide molecules in the two leaflets do not present area exclusion to each other. Here, we

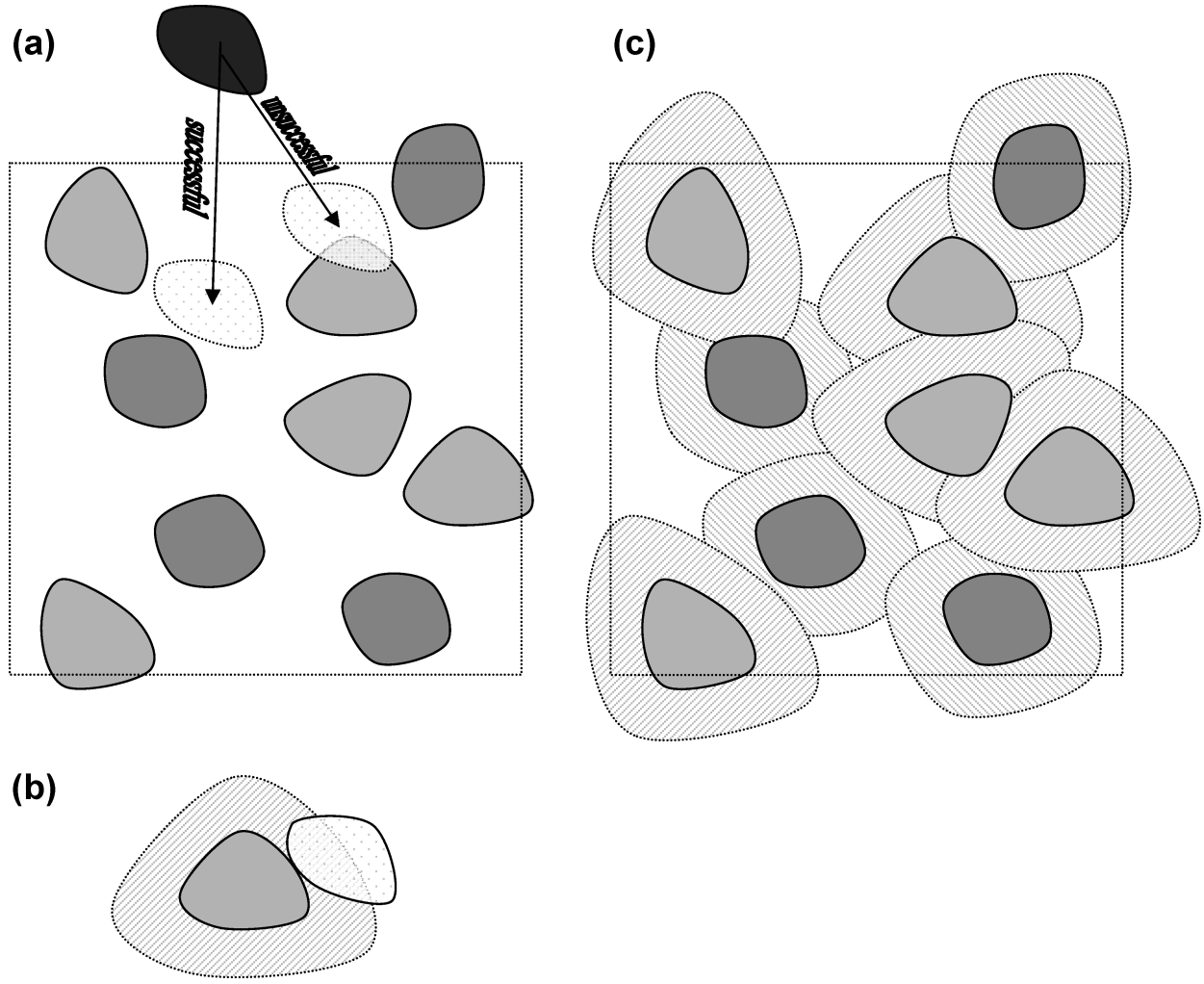

Figure 2. Area exclusion of proteins within a membrane. (a) Placement of a test molecule into a distribution of crowders. A placement is successful when no overlap with any crowder occurs and unsuccessful otherwise. (b) The region excluded to a test molecule by a crowder. This region is larger than the original cross section of the crowder. The expanded region is shown as hatched. (c) Overlap of excluded regions of crowders. Due to their overlap, the total filled area is less than the sum of all of the excluded regions. Note that the fraction of area unfilled by the excluded region of any crowder is the desired quantity f, but there is no simple way to calculate the total filled or unfilled area.

consider the situation where the membrane is symmetric with respect to the two leaflets so that the in-plane species can be present in both leaflets with equal probability. Throughout this article, we stipulate that "in" refers to the in-plane species on one leaflet of the membrane. In particular, c_{in} denotes the density of the in-plane species in one leaflet; the total density of the in-plane species is thus $2c_{in}$. Accordingly, eq 9 for the total density of bound peptide becomes

$$c = c_{tr} + 2c_{in} \tag{14}$$

No modification is required for eqs 10−13. Now, eq 7 assumes that each protein molecule presents area exclusion to every other protein molecule. It can be used directly to calculate $\Delta\mu_{in}$, the increase in chemical potential of the in-plane species in one leaflet due to the crowding with itself and with the transmembrane species, present at densities c_{in} and c_{tr}, respectively. On the other hand, the transmembrane species experiences self-crowding and crowding by the in-plane species from both leaflets. To use eq 7 to calculate $\Delta\mu_{tr}$, we assume that, in addition to the transmembrane species, at density c_{tr}, there is a single in-plane species, at density ηc_{in}, with $1 < \eta < 2$ to account for the fact that peptide molecules on the two leaflets are not mutually exclusive (see the Appendix for further discussion).

The partitioning of a peptide known as LAH_4W_4 between the transmembrane and in-plane orientations was studied by Aisenbrey et al.[16] The peptide, with the sequence KKALLA-WALHHLAW-LAHWLAWHLKKA, was helical in either orientation in bilayers of the lipid 1-palmitoyl-2-oleoyl-*sn*-glycero-3-phosphocholine (POPC). The partitioning between the two orientations was pH-dependent. The dominant species was the in-plane orientation at pH 4 but became the transmembrane species at pH 7. The two orientations coexisted at pH 5. Figure 3 shows their data for the fractions p_α, α = tr and in, of transmembrane and in-plane peptides as functions of the lipid-to-bound-peptide ratio x. This ratio is inversely proportional to the density of bound peptide

$$x = \frac{1}{s_{lip}c} \tag{15}$$

where $s_{lip} \sim 30$ Å^2 is the area projected per lipid molecule.[27] At very low densities of bound peptide, the ratio p_{in}/p_{tr} is 3.5 to 1. As the density of bound peptide increases, the curves for p_{in}

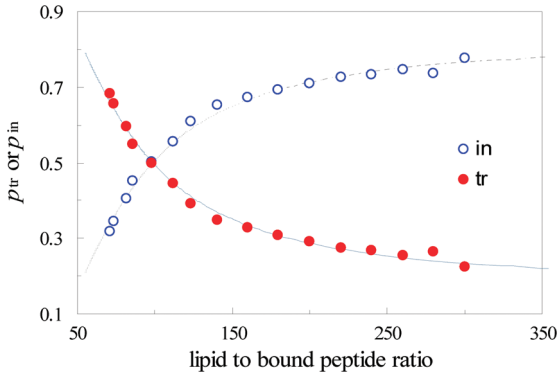

Figure 3. Partitioning of membrane-bound peptide into transmembrane and in-plane orientations. Symbols present data of Aisenbrey et al.[16] at pH = 5. The curves are calculated according to eq A5, with parameters given in the text and details given in the Appendix.

and p_{tr} cross over. At the high end of the experimental density range, p_{in}/p_{tr} decreases to 0.5. A simple explanation of the crossover is that, at high densities of bound peptide, the two species compete for surface area. The in-plane species, with a larger cross section, becomes less and less favorable.

As Figure 3 shows, the data of Aisenbrey et al. can be fitted to eq 7 with the cross section of the transmembrane species modeled as a circle (with radius a) and the cross section of the in-plane species modeled as a rectangle (with width $2a$ and length L). With $\eta = 1.5$ (to account for the in-plane species' simultaneous presence in the two leaflets), the fitting parameters are $a = 8.1$ Å, $L = 115$ Å, and $K_{o0} = 0.37$. The value for the length of the in-plane species appears to be unrealistically large for a 26 residue helical peptide but is demanded by the sharp decrease in p_{in} as the lipid-to-bound-peptide ratio decreases from 300 to 70. Aisenbrey et al. also fitted their data to eq 7 but modeled the cross sections of both the transmembrane and the in-plane species as circles. The fitted values of the radii were 11 and 35 Å, respectively. The corresponding area of the in-plane species is twice what we obtain using a rectangle model and is thus even more unrealistic.[28]

The unrealistically large cross section of the in-plane species required to fit the data suggests that an alternative model may be needed. As discussed below, molecular dynamics simulations show that the transmembrane species, but not the in-plane species, can form a dimer, trimer, and tetramer (Yi and Zhou, unpublished). Oligomerization of the transmembrane species would reduce the area excluded to other peptide molecules and thus lower its chemical potential. Consequently, the increase in p_{tr} with decreasing lipid-to-bound-peptide ratio would be steeper than that predicted from a monomer-only model; thereby, a smaller value of L would be required to fit the data.

Redistribution within a Membrane by an External Field

As noted in the Introduction, density variations of membrane proteins among different parts of a cell membrane can have a significant influence on crowding effects. In particular, protein compositions in different lipid rafts and in nonraft regions may be significantly different. For a membrane protein carrying a net charge, an applied electric field (E) can cause such a variation in density. If the cell is modeled a sphere (with radius $\mathcal{R}$) and the electric field is directed from the north pole to the south pole, the variation in density corresponds to an effective potential energy[29]

$$U(\theta) = \beta \cos\theta \tag{16}$$

where θ is the polar angle. The prefactor β is given by $\gamma mE\mathcal{R}/D$, where γ is a numerical factor ($\sim$1.5), m is the mobility of the membrane protein, and D is its diffusion constant. Both m and D can be affected by crowding, but their ratio should mainly be determined by the distribution of charges on the protein molecule; if the membrane protein is treated as a point charge, then m/D equals the net charge of the protein. In the case where $\beta > 0$ (for a protein carrying a positive charge), the electric field will drive the protein toward the south pole. However, the density there will be limited by crowding effects; hence, the density variation will be more moderate than predicted by the Boltzmann distribution corresponding to the energy function of eq 16. Qualitatively, this predicted behavior is consistent with the observations of Ryan et al.[14] We now show that their data can be fitted by accounting for crowding according to eq 7.

We assume that all of the membrane proteins in the cell studied by Ryan et al. have approximately the same cross section, to be modeled as a circle with radius a. Let the total density of the membrane proteins at polar angle be $c(\theta)$. Then crowding-induced increase in chemical potential of a single tagged protein molecule is given by

$$\frac{\Delta\mu(\theta)}{k_BT} = -\ln[1 - \phi(\theta)] + \frac{3\phi(\theta)}{1 - \phi(\theta)} + \left[\frac{\phi(\theta)}{1 - \phi(\theta)}\right]^2 \tag{17}$$

where $\phi(\theta) = \pi a^2 c(\theta)$. Both the potential energy due to the interaction with the applied electric field and the increase in chemical potential due to crowding affect the density of the membrane proteins at a given polar angle, through

$$c(\theta) = Ae^{-[U(\theta)+\Delta\mu(\theta)]/k_BT} \tag{18}$$

Here, A is a constant that is determined by the total number of membrane proteins in the cell.

We represent the density profile by the values of $\phi(\theta)$ at $N = 101$ points uniformly spaced between $\cos\theta = -1$ and 1. Using index n to denote these discrete points, eq 18 can be transformed to

$$\phi_n = \langle\phi\rangle \frac{e^{-(U_n+\Delta\mu_n)/k_BT}}{\frac{1}{N}\sum_{n=1}^{N} e^{-(U_n+\Delta\mu_n)/k_BT}} \tag{19}$$

where $\langle\phi\rangle$ is the average area fraction, which would be the value of ϕ everywhere if the electric field were turned off. Equation 19 involves two parameters, β and $\langle\phi\rangle$.[30] Ryan et al.[14] made measurements at four field strengths, 5, 10, 15, and 20 V/cm. Their data can be fitted with $\langle\phi\rangle = 0.2$ and $\beta/k_BT = 0.84$, 1.19, 1.90, and 2.18, respectively, at these four field strengths. Figure 4 displays a comparison between the calculation and the experimental data for field strengths of 5 and 20 V/cm.

Partitioning between Membrane and Solution Phases

Usually, a protein that is found in the membrane phase also has a fraction in the solution phase. Following Minton,[8−10] we now consider the partitioning of such a protein between the two phases (Figure 1b). The surface density c of the membrane-bound fraction and the concentration C_s in the solution satisfy the following mass conservation equation

$$cs_{\mathrm{lip}}C_{\mathrm{lip}} + C_{\mathrm{s}} = C \tag{20}$$

where C_{lip} is the lipid concentration and C is the total concentration of the protein.

Consider the case where the membrane-bound fraction consists of several species, referred to by index α, and the fraction in the solution is a single species. In analogy to eq 13, the equilibrium between species α and the solution species is governed by

$$\frac{c_\alpha}{C_{\mathrm{s}}} = \frac{\Lambda_\alpha}{\Lambda_{\mathrm{s}}} \mathrm{e}^{-(\Delta\mu_\alpha - \Delta\mu_{\mathrm{s}})/k_{\mathrm{B}}T} \tag{21a}$$

As seen above, the crowding-induced increase in chemical potential, $\Delta\mu_\alpha$, in the membrane phase depends on the density c_α of species α. On the other hand, we assume that the excess chemical potential $\Delta\mu_{\mathrm{s}}$ of the protein in the solution to be independent of protein concentration since, as noted in the Introduction, the concentration of a single protein species in the solution phase is typically low. We thus can write

$$\frac{c_\alpha}{C_{\mathrm{s}}} = K_{\alpha 0} \mathrm{e}^{-\Delta\mu_\alpha/k_{\mathrm{B}}T} \tag{21b}$$

where $K_{\alpha 0}$ is the membrane binding constant for species α in the dilute limit. In particular, adding crowding agents in the solution phase will increase $\Delta\mu_{\mathrm{s}}$ and hence $K_{\alpha 0}$ uniformly for every membrane-bound species, leading to an increase in the membrane-bound fraction.[31]

Note that by specializing eq 21b to two different membrane-bound species and taking the ratio of the resulting equations, we arrive at a relation governing the equilibration between the two species. An example of such a relation is eq 13 for the equilibration between the transmembrane and in-plane species of a membrane-bound peptide. Here, we further consider the partitioning of the peptide between the membrane and solution phases. The fractions of the two membrane-bound species out of the total peptide concentration are given by

$$P_{\mathrm{tr}} = p_{\mathrm{tr}}(1 - C_{\mathrm{s}}/C) \qquad P_{\mathrm{in}} = p_{\mathrm{in}}(1 - C_{\mathrm{s}}/C) \tag{22}$$

We now need to specify the membrane binding constants K_{tr0} and K_{in0} of both species, not just their ratio (given by K_{o0}). As shown in Figure 5, the data of Aisenbrey et al.[16] for P_{tr} and P_{in} of the LAH_4W_4 peptide can be fitted with the additional parameter $\pi a^2 K_{\mathrm{tr0}} = (27.5\ \mu\mathrm{M})^{-1}$; the other parameters are as reported for Figure 3.

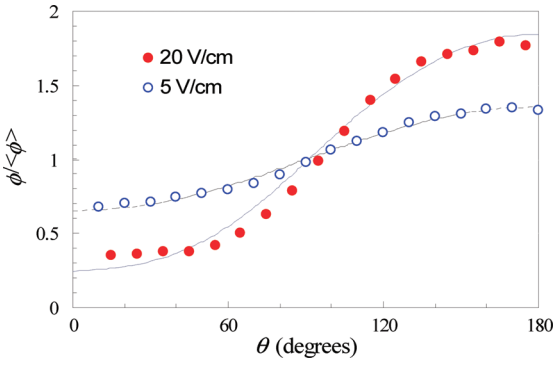

Figure 4. Redistribution of membrane proteins within a cell membrane by an electric field. Symbols present data of Ryan et al.[14] The curves are calculated according to eq 19, with parameters, given in the text, optimized by a systematic search. For a given set of parameters, the area fraction ϕ is obtained by iteration.

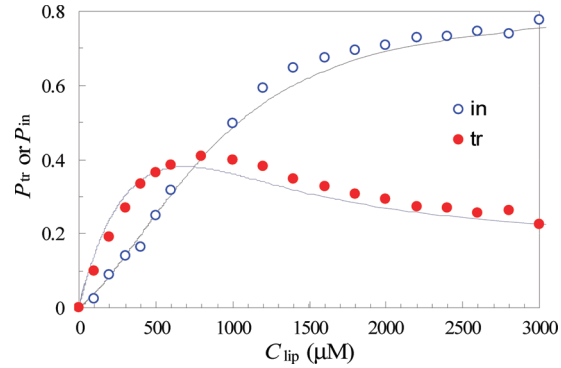

Figure 5. Partitioning of the LAH_4W_4 peptide between the membrane and solution phases. Symbols present data of Aisenbrey et al.[16] at pH = 5. The curves are calculated according to eq A5, with parameters given in the text, and details given in the Appendix.

Oligomerization within a Membrane: Equilibria

Up to now, we have only considered equilibration between monomeric species. The effects of crowding on oligomerization equilibria have been analyzed in a number of theoretical studies.[7,8,10,11] In a recent study of the membrane binding of lysozyme, Gorbenko et al.[15] invoked self-association to fit their binding data. As mentioned above, molecular dynamics simulations show that the LAH_4W_4 peptide, while in the transmembrane orientation, can form a dimer, trimer, and tetramer (Yi and Zhou, unpublished). We now examine the equilibria between these species under crowding.

Let the monomeric and dimeric species of a membrane protein be denoted with indices 1 and 2, respectively. Two protein molecules in the monomeric state form a single copy of the dimeric species. In analogy to eq 10, the equilibrium between the two species is governed by

$$\mu_2 = 2\mu_1 \tag{23}$$

This relation can be transformed to (cf. eq 13)

$$\frac{c_2}{{c_1}^2} = \frac{\Lambda_2}{{\Lambda_1}^2} \mathrm{e}^{-(\Delta\mu_2 - 2\Delta\mu_1)/k_{\mathrm{B}}T} = K_{20} \mathrm{e}^{-(\Delta\mu_2 - 2\Delta\mu_1)/k_{\mathrm{B}}T} \tag{24}$$

where K_{20} is the dimerization constant in the dilute limit.

Generalization to the formation of higher oligomers is given by eq A2 of the Appendix. There, we describe how the densities of the various oligomeric species can be obtained. For the LAH_4W_4 peptide, in addition to the monomer, dimer, trimer, and tetramer species in the transmembrane orientation, there is also a monomer species in the in-plane orientation. Just as before, we model the cross sections of the monomer species in the two orientations as a circle and a rectangle, respectively. The models for the higher transmembrane oligomers are illustrated in Figure 6a.

The data of Aisenbrey et al.[16] for the partitioning between the transmembrane and in-plane orientations of the membrane-bound LAH_4W_4 peptide, already shown in Figure 3, can also be fitted to the present model involving higher oligomers in

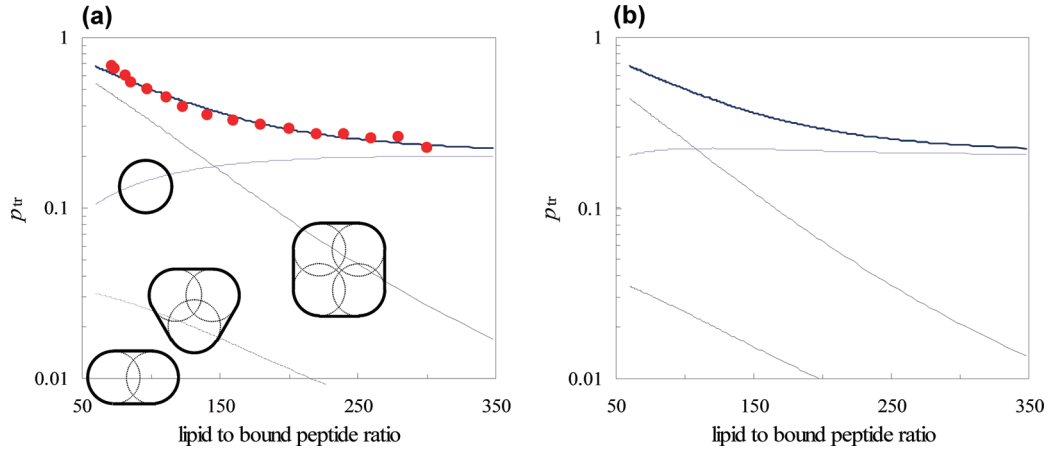

Figure 6. Partitioning of the LAH_4W_4 peptide between the transmembrane monomer, dimer, trimer, tetramer, and in-plane monomer. Symbols in (a) present data of Aisenbrey et al.[16] at pH = 5 for the total transmembrane fraction out of the membrane-bound peptide. The top curve is the counterpart calculated according to eqs A5 and A6. The three lowers curves are the contributions of the monomer, trimer, and tetramer; the contribution of the dimer is too low on the scale shown. The cross sections of the four oligomers are illustrated. The curves in (b) are calculated by turning off crowding and then are rescaled to produce the same total transmembrane fraction as that in (a). The parameters of the calculations are given in the text, and details are given in the Appendix.

the transmembrane orientation. As expected earlier, a much more realistic value, $L = 40$ Å, for the length of the 26 residue helical peptide can now be used. As shown in Figure 6a, the data for p_{tr} can be fitted by selecting $(\pi a^2)^{-i} s_i K_{i0} = 10^{-1}$, 10^3, and 10^6 for the equilibrium constants for forming the successively higher oligomers, expressed in dimensionless units, along with $a = 8$ Å and $K_{o0} = 0.5$.

Figure 6a also displays the contributions to p_{tr} by the individual oligomeric species. As the total density of bound peptide increases, the population shifts from monomer to tetramer (with the dimer and trimer always at much lower densities). Interestingly, in molecular dynamics simulations, transmembrane dimers and trimers of the LAH_4W_4 peptide were formed only transiently, but tetramers were stable (Yi and Zhou, unpublished). The shift from monomer to tetramer is much more rapid than expected from the oligomerization constants K_{i0} in the dilute limit (see Figure 6b). Crowding favors higher oligomers and shifts the equilibrium toward their formation. This provides an explanation for the observation that oligomerization enhances the partitioning of some membrane proteins into lipid rafts, which presumably are more crowded than nonraft regions.[18,32−34]

Oligomerization within a Membrane: Kinetics

Not only the equilibria but also the kinetics of oligomerization of membrane proteins play central roles in biological processes such as signal transduction. As in the solution phase, crowding in the membrane phase can affect, in opposite directions, two determinants of the oligomerization rate.[2,3,35] The crowding-induced shift of equilibrium toward oligomerization is equivalent to an attractive potential,[2,36] which increases the oligomerization rate. On the other hand, crowding also slows down the diffusion of the monomeric species, thereby decreasing the oligomerization rate. These features are observed in recent Monte Carlo simulations of the diffusion-controlled activation of transducin by a single photoactivated rhodopsin molecule within a high density of other rhodopsin molecules.[13] The simulation protocol used for this membrane-bound system is very similar to what was used in one of the earliest simulation studies on the effects of crowding on the binding rate.[36] In that study, we were also able to fit the simulation results by modifying the Smoluchowski theory for diffusion-controlled reactions to account for crowding effects. We now present a two-dimensional version of the theory and use it to analyze the simulation results of Dell'Orco and Schmidt.[13]

In the system simulated by Dell'Orco and Schmidt, the photoactivated rhodopsin molecule and surrounding transducin molecules are reactants, and the other rhodopsin molecules can be considered as crowders. We follow Szabo's formulation[37] of the Smoluchowski theory, in which the many-body problem is reduced to the reaction between a single pair of reactant molecules modeled as circular disks. The crowders induce an effective potential, $U_{cr}(r)$, between the reactant molecules [in principle, $U_{cr}(r)$ can be obtained from a scaled particle theory by treating the pair of reactant molecules at a particular distance r as a new species]. In addition, they reduce the relative diffusion constant of the reactant molecules from D_0 to D. The diffusion-controlled reaction between the pair of molecules is described by a time-dependent rate coefficient $k(t)$, which is governed by the Smoluchowski equation and has a complicated dependence on $U_{cr}(r)$. In the absence of crowders, $U_{cr}(r) = 0$ and $D = D_0$, the rate coefficient is given by

$$k_0(t) = \frac{8D_0}{\pi} \int_0^\infty \frac{\exp[^{-D_0 t \xi^2/a^2} \mathrm{d}\xi]}{\xi[J_0^2(\xi) + Y_0^2(\xi)]} \qquad (25)$$

where a is the contact distance between the reactant molecules, and $J_0(\xi)$ and $Y_0(\xi)$ are Bessel functions. In the presence of the transducin molecules at a density c, the survival probability of the photoactivated rhodopsin molecule is given by

$$S(t) = \mathrm{e} - c \int_0^t k(t')\mathrm{d}t' \qquad (26)$$

If simulations are started from an equilibrium distribution of the transducin molecules and followed up to time t_{cut}, then their mean first encounter time with the photoactivated rhodopsin molecule is obtained as

$$\tau(t_{cut}) = \int_0^{t_{cut}} S(t)\mathrm{d}t \qquad (27)$$

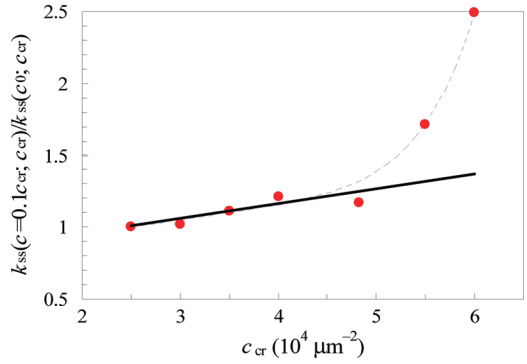

Figure 7. Influence on the steady-state rate constant k_{ss} by a crowding-induced effective potential. Symbols are calculated from the simulation data of Dell'Orco and Schmidt;[13] the dashed curve is just for guiding the eye. The solid line is calculated according to eq 29 for the case $U_{cr}(r) = 0$, with πa^2, the area inaccessible to a transducin molecule, set to 4 nm × 4 nm to mimic the simulated system.

One can use the long-time limit $\lim_{t_{cut}\to\infty} \tau(t_{cut})$, denoted simply as τ, to define a steady-state rate constant

$$k_{ss} = \frac{1}{\tau c} \tag{28}$$

Note that k_{ss} is not simply the long-time limit of $k(t)$ [in fact, $\lim_{t\to\infty} k(t) \to 0$]. It is proportional to D but, like $k(t)$, has a complicated dependence on $U_{cr}(r)$. In the absence of crowders, $U_{cr}(r) = 0$; the corresponding steady-state rate constant k_{ss0} can be calculated to high accuracy from an approximate relation

$$\frac{k_{ss0}}{2\pi D_0} \equiv y = \frac{\chi K_1(\chi)}{K_0(\chi)} \tag{29}$$

where $\chi = (2\pi a^2 cy)^{1/2}$ and $K_0(\chi)$ and $K_1(\chi)$ represent modified Bessel functions.

Dell'Orco and Schmidt obtained results for τ with the crowders modeled in three different ways, as randomly disbursed mobile monomers, as an immobilized periodic array of dimers, and as immobilized random blocks of dimers. Their simulations confirmed that the crowders reduce the diffusion constants of the reactant molecules and that k_{ss} is proportional to D. Extensive data were presented for the first way of modeling the crowders, which we now analyze within the Smoluchowski theory outlined above. These data consist of results for τ for two sets of transducin and crowder densities; the latter will now be denoted as c_{cr}. In both sets, c_{cr} increased from 2.5 × 10^4 to 6 × 10^4 μm^{-2}, but in the first set, c increased in proportion to c_{cr} ($c = 0.1c_{cr}$), whereas in the second set, c was fixed at 2.5 × 10^3 μm^{-2} (to be referred to as c_0). To isolate the effect of the crowding-induced effective potential [i.e., $U_{cr}(r)$], in Figure 7, we plot $k_{ss}(c = 0.1c_{cr};c_{cr})/k_{ss}(c_0;c_{cr})$ calculated from the simulation results as a function of c_{cr}. For comparison, we also plot the corresponding results obtained from eq 29 for the case $U_{cr}(r) = 0$. As c_{cr} increases from 2.5 × 10^4 to 6 × 10^4 μm^{-2} (corresponding to an increase in area fraction from 0.23 to 0.54), $k_{ss}(c = 0.1c_{cr};c_{cr})/k_{ss}(c_0;c_{cr})$ becomes significantly higher than that predicted without $U_{cr}(r)$. While the unavailability of $U_{cr}(r)$ and the complicated dependence of k_{ss} on $U_{cr}(r)$ preclude a quantitative prediction for the effect of the crowding-induced effective potential, the trend of the deviation of $k_{ss}(c = 0.1c_{cr};c_{cr})/k_{ss}(c_0;c_{cr})$ from the counterpart with $U_{cr}(r) = 0$ is consistent with the expected effect of $U_{cr}(r)$.

Real proteins form stereospecific complexes rather than a nonspecific complex as modeled by the Smoluchowski theory. The stereospecificity further complicates the dependence of k_{ss} on the crowding-induced effective potential. There is significant progress in modeling the influence of interaction potentials on the diffusion-controlled rates for stereospecific binding in three dimensions.[35] It will be interesting to see to what extent the three-dimensional results are helpful for developing theories in two dimensions.

When oligomerization is activation-controlled rather than diffusion-controlled, crowding always enhances the rate of oligomerization.[3] Membrane binding has been observed to kinetically accelerate the aggregation of amyloidogenic peptides.[38−41] It has been recognized that the membrane environment enhances the propensity of secondary structure, which precedes aggregation, and that the reduction in dimensionality from three to two upon membrane binding increases the local peptide concentration and promotes oligomerization.[42] We can now propose crowding as the third contributing factor to the aggregation-accelerating effect of membrane binding.

Outlook

In this article, we have highlighted the fact that membrane proteins, due to the reduction from three to two in the dimensionality of the space in which they are located, are especially prone to crowding. In addition, a number of processes that are distinct to the membrane environment, such as equilibration between membrane orientations and redistribution within a cell membrane, are subject to crowding effects. It is clear that membrane crowding deserves greater attention, and we hope that this article will spur new efforts toward its study.

We end with the following remarks:

1. In studying processes in cell membranes, one should be cognizant of potential crowding effects. A rule of thumb is that when the ratio of lipid molecules to total protein molecules is 100 or less, crowding effects may come into play.

2. When developing theories for membrane processes, crowding should be taken into consideration.

3. It might be worthwhile to re-examine previous experimental studies to look for crowding effects.

4. The scaled particle theory used in the analyses here may have limitations. The theory as applied to crowding effects does not explicitly treat the solvent. It has been more thoroughly interrogated in the solution phase,[21−25] where the solvent, that is, water, is much smaller in size relative to protein molecules under study as well as other macromolecular crowders. In the membrane phase, the solvent consists of lipid molecules; their size is much closer to peptides and protein molecules under study. In addition, in the two-dimensional version as applied to membrane crowding, the membrane proteins are represented by their cross sections; for proteins with varying cross sections along the membrane depth, this approximation presents ambiguity.[17]

5. Besides area exclusion, other types of interactions such as charge−charge interactions[43] can also be dependent on protein concentration.

6. In addition to equilibrium properties, membrane crowding influences kinetic properties. Theories will be valuable to predict magnitudes and trends of such influences.

Acknowledgment. This work was supported, in part, by NIH Grant GM058187.

Appendix

Here, we present technical details for the calculations presented in Figures 3, 5, and 6. We consider the general case where a peptide can partition between the solution phase and the membrane phase. In the former phase, the peptide is a single monomeric species, to be referred to with index "s", but in the latter phase, the peptide consists of several species with different membrane orientations and oligomeric states. In the in-plane orientation, the peptide is monomeric and can occupy either leaflet with equal probability. This membrane species will be referred to with index 0. In the transmembrane orientation, the peptide can be a monomer, dimer, trimer, or tetramer, to be referred to with indices 1−4, respectively.

The equilibration between either of the monomeric membrane species with the solution species is governed by (see eq 21b)

$$c_i = K_{i0} C_s \mathrm{e}^{-\Delta\mu_i/k_B T} \tag{A1}$$

where $i = 0$ or 1. Note that c_0 is the density of the in-plane species in one leaflet. The equilibration between the transmembrane monomer and a higher transmembrane oligomer is governed by (see eq 24)

$$c_i = K_{i0} {c_1}^i \mathrm{e}^{-(\Delta\mu_i - i\Delta\mu_1)/k_B T} \tag{A2}$$

where $i = 2$, 3, or 4. We work with dimensionless quantities. The densities c_i are substituted by the area fractions ϕ_i through the relation

$$\phi_i = s_i c_i \tag{A3}$$

where s_i are the areas of species i. In addition, we express s_i in units of the area of species 1, which is a circle with radius a

$$s_i = \pi a^2 \sigma_i \tag{A4}$$

By definition, $\sigma_1 = 1$. Equations A1 and A2 can now be transformed to

$$\phi_i = \pi a^2 \sigma_i K_{i0} C_s \mathrm{e}^{-\Delta\mu_i/k_B T} \qquad i = 0, 1 \tag{A5}$$

$$\phi_i = (\pi a^2)^{-i+1} \sigma_i K_{i0} {\phi_1}^i \mathrm{e}^{-(\Delta\mu_i - i\Delta\mu_1)/k_B T} \qquad i = 2, 3, 4 \tag{A6}$$

To solve for ϕ_i, $i = 0$−4, we need to specify the free-energy increases $\Delta\mu_i$ due to crowding. The in-plane species in each leaflet competes with the four transmembrane species for surface area and is not affected by the in-plane species on the other leaflet. According to eq 7, we have

$$\mathrm{e}^{-\Delta\mu_0/k_B T} = (1 - \phi) \exp\left[-\frac{l_0 c_l/2\pi + s_0 c}{1 - \phi} - \frac{s_0 {c_l}^2/4\pi}{(1 - \phi)^2}\right] \tag{A7}$$

where

$$\phi = \sum_{i=0}^{4} \phi_i \tag{A8}$$

In analogy to eq A4, we express the circumferences of species i in units of $l_1 = 2\pi a$

$$l_i = 2\pi a \lambda_i \tag{A9}$$

Then, the terms of eq A7 can be expressed in terms of dimensionless quantities as

$$l_0 c_l/2\pi = 2\lambda_0 \sum_{i=0}^{4} \frac{\lambda_i \phi_i}{\sigma_i} \tag{A10}$$

$$s_0 c = \sigma_0 \sum_{i=0}^{4} \frac{\phi_i}{\sigma_i} \tag{A11}$$

$$s_0 {c_l}^2/4\pi = \sigma_0 \left(\sum_{i=0}^{4} \frac{\lambda_i \phi_i}{\sigma_i}\right)^2 \tag{A12}$$

On the other hand, the transmembrane species compete against the in-plane species in both leaflets for surface area. The fact that the two in-plane species do not present area exclusion to each other complicates the calculation of $\Delta\mu_i$ for $i = 1$−4. We can bracket the effect of the in-plane species in the two leaflets on the transmembrane species by two extreme situations. In one extreme, only the in-plane species in one leaflet is present; in the other extreme, both in-plane species are present and present area exclusion to each other. In the latter situation, the effect of the two in-plane species on the transmembrane species can be accounted for by assuming only one in-plane species but counting that species twice or doubling the density c_0. With these considerations, we assume that the effect of the in-plane species in the two leaflets on the transmembrane species can be accounted for by assuming an effective density ηc_0, where η is between 1 and 2. The results for $\Delta\mu_i$, $i = 1$−4, are given by

$$\mathrm{e}^{-\Delta\mu_i/k_B T} = (1 - \phi') \exp\left[-\frac{l_i c_l'/2\pi + s_i c'}{1 - \phi'} - \frac{s_i {c_l'}^2/4\pi}{(1 - \phi')^2}\right] \tag{A13}$$

where

$$\phi' = \eta\phi_0 + \sum_{j=1}^{4} \phi_j \tag{A14}$$

$$l_i c_l'/2\pi = 2\lambda_i\left(\frac{\lambda_0\eta\phi_0}{\sigma_0} + \sum_{j=1}^{4}\frac{\lambda_j\phi_j}{\sigma_j}\right) \quad \text{(A15)}$$

$$s_i c' = \sigma_i\left(\frac{\eta\phi_0}{\sigma_0} + \sum_{j=1}^{4}\frac{\phi_j}{\sigma_j}\right) \quad \text{(A16)}$$

$$s_i c_l'^2/4\pi = \sigma_i\left(\frac{\lambda_0\eta\phi_0}{\sigma_0} + \sum_{j=1}^{4}\frac{\lambda_j\phi_j}{\sigma_j}\right)^2 \quad \text{(A17)}$$

In all of the calculations presented in Figures 3, 5, and 6, we choose $\eta = 1.5$.

We now discuss details specific to Figure 3. In this case, the peptide exists only as a monomer in the transmembrane orientation; species 0 and 1 can be identified with in and tr, respectively. Their equilibration is governed by eq A5. In the present case, the solution species could be eliminated, but we choose to use it as a convenient intermediary between the two membrane-bound species. At given values of a, L, and $K_{tr0}/K_{in0} = K_{o0}$, we solve eq A5 by iteration for p_{tr} and p_{in} at increasing values of the lipid-to-bound-peptide ratio. Specifically, the value of the prefactor, $\pi a^2 K_{tr0} C_s$, in eq A5, is increased from 0 to 0.3 at an increment of 10^{-3}. At each step, ϕ_{tr} and ϕ_{in} are repeatedly evaluated by eq A5 using results from the preceding iteration as input. The iteration is considered converged when the changes in ϕ_{tr} and ϕ_{in} fall below a threshold, set at a relative change of 10^{-4}. The values of ϕ_{tr} and ϕ_{in} thus obtained are then converted to the densities of the transmembrane and in-plane species (eq A3). Finally, the lipid-to-bound-peptide ratio x is calculated according to eq 15, and the transmembrane and in-plane fractions are calculated as

$$p_{tr} = \frac{c_{tr}}{c_{tr} + 2c_{in}} \qquad p_{in} = \frac{2c_{in}}{c_{tr} + 2c_{in}} \quad \text{(A18)}$$

where the factor of 2 accounts for the fact that the in-plane species is present on both leaflets of the membrane (see eq 14). To fit the data of Aisenbrey et al.,[16] the values of a, L, and K_{o0} are varied systematically; values corresponding to the best agreement are reported in the text.

The calculations that produce the curves in Figure 3 also yield the curves in Figure 5. It should be recalled that, for the former curves, each point corresponds to a particular value of $\pi a^2 K_{tr0} C_s$. Now, we need to separately specify K_{tr0} in order to find the corresponding value of C_s. Then, the lipid concentration is (eq 20)

$$C_{lip} = \frac{1}{cs_{lip}}(C - C_s) = x(C - C_s) \quad \text{(A19)}$$

where C is the total peptide concentration, equal to 10 μM in the experiments of Aisenbrey et al.[16] The fractions of the transmembrane and in-plane species out of the total peptide concentration are given by eq 22. To achieve the best agreement with the experimental data of Aisenbrey et al. for P_{tr} and P_{in}, we systematically vary the value of $\pi a^2 K_{tr0}$. The optimized value is reported in the text.

The curves in Figure 6 are obtained by iterating eqs A5 and A6. As illustrated in Figure 6a, the cross section of the dimer is defined by placing two circular monomers at a center-to-center distance of $d = 1.5a$. The two external tangents then complete the perimeter. Similarly, the cross sections of the trimer and tetramer are defined by placing three monomers at the vertices of an equilateral triangle and a square, respectively, both with side length d. Again, external tangents round out the respective perimeters. The circumferences of the three oligomers are

$$l_i = 2\pi a + id \quad \text{(A20)}$$

for $i = 2$, 3, and 4. Their areas are

$$s_i = \pi a^2 + iad + \gamma_i d^2 \quad \text{(A21)}$$

with $\gamma_i = 0$, $3^{1/2}/4$, and 1, respectively, for $i = 2$, 3, and 4. Upon fixing a, the radius of the transmembrane monomer (and the half-width of the in-plane monomer), at 8 Å and L, the length of the in-plane monomer, at 40 Å, we systematically vary K_{o0} and the prefactors $(\pi a^2)^{-i+1}\sigma_i K_{i0} = (\pi a^2)^{-i} s_i K_{i0}$ in eq A6 to achieve the best agreement with the data of Aisenbrey et al.,[16] for p_{tr} and p_{in}. In the present model, we have

$$p_{tr} = \frac{c_1 + 2c_2 + 3c_3 + 4c_4}{2c_0 + c_1 + 2c_2 + 3c_3 + 4c_4}$$
$$p_{in} = \frac{2c_0}{2c_0 + c_1 + 2c_2 + 3c_3 + 4c_4} \quad \text{(A22)}$$

The iteration of eqs A5 and A6 is very similar to what is described above for the monomer-only model. Here, $\pi a^2 K_{tr0} C_s$ in eq A5 is increased from 0 to 0.03 at an increment of 10^{-4}. In the calculation for Figure 6b, crowding is turned off for the oligomerization equilibria by setting $\Delta\mu_i$ to 0 for $i = 2-4$. In order to compare against Figure 6a, we scale the contributions of the four oligomeric states so that the total transmembrane fraction is the same as that in Figure 6a for a given lipid-to-bound-peptide ratio.

References and Notes

(1) Hall, D.; Minton, A. P. *Biochim. Biophys. Acta* **2003**, *1649*, 127.
(2) Zhou, H.-X. *J. Mol. Recognit.* **2004**, *17*, 368.
(3) Zhou, H.-X.; Rivas, G.; Minton, A. P. *Annu. Rev. Biophys.* **2008**, *37*, 375.
(4) Alberts, B.; Johnson, A.; Lewis, J.; Raff, M.; Roberts, K.; Walter, P. *Molecular Biology of the Cell*, 4th ed; Garland Science: New York, 2002.
(5) Dupuy, A. D.; Engelman, D. M. *Proc. Natl. Acad. Sci. U.S.A.* **2008**, *105*, 2848.
(6) Zimmerman, S. B.; Trach, S. O. *J. Mol. Biol.* **1991**, *222*, 599.
(7) Grasberger, B.; Minton, A. P.; DeLisi, C.; Metzger, H. *Proc. Natl. Acad. Sci. U.S.A.* **1986**, *83*, 6258.
(8) Chatelier, R. C.; Minton, A. P. *Biophys, J.* **1996**, *71*, 2367.
(9) Minton, A. P. *Biophys, J.* **1999**, *76*, 176.
(10) Minton, A. P. *Biophys. Chem.* **2000**, *86*, 239.
(11) Zuckermann, M. J.; Heimburg, T. *Biophys. J.* **2001**, *81*, 2458.
(12) Woolf, P. J.; Linderman, J. J. *Biophys. Chem.* **2003**, *104*, 217.
(13) Dell'Orco, D.; Schmidt, H. *J. Phys. Chem. B* **2008**, *112*, 4419.
(14) Ryan, T. A.; Myers, J.; Holowka, D.; Baird, B.; Webb, W. W. *Science* **1988**, *239*, 61.
(15) Gorbenko, G. P.; Ioffe, V. M.; Kinnunen, P. K. J. *Biophys. J.* **2007**, *93*, 140.
(16) Aisenbrey, C.; Bechinger, B.; Grobner, G. *J. Mol. Biol.* **2008**, *375*, 376.
(17) In reality, different cross sections of a membrane protein are obtained when it is sliced at different depths into the membrane. This is true, for example, of a protein with a small transmembrane domain but a large intracellular or extracellular domain. Dell'Orco and Schmidt[13] modeled such a case by using two cross sections, one for the transmembrane domain and one for the extracellular domain. Here, we neglect this complication

and simply take a "typical" cross section as the two-dimensional representation of the membrane protein.

(18) Simons, K.; Vaz, W. L. *Annu. Rev. Biophys. Biomol. Struct.* **2004**, *33*, 269.

(19) Hanzal-Bayer, M. F.; Hancock, J. F. *FEBS Lett.* **2007**, *581*, 2098.

(20) Lebowitz, J. L.; Helfand, E.; Praestgaard, E. *J. Chem. Phys.* **1965**, *43*, 774.

(21) Minton, A. P. *Mol. Cell. Biochem.* **1983**, *55*, 119.

(22) Minton, A. P. *Methods Enzymol.* **1998**, *295*, 127.

(23) Rivas, G.; Fernandez, J. A.; Minton, A. P. *Proc. Natl. Acad. Sci. U.S.A.* **2001**, *98*, 3150.

(24) Liu, Z.; Weng, W.; Bookchin, R. M.; Lew, V. L.; Ferrone, F. A. *Biophys. J.* **2008**, *94*, 3629.

(25) Yuan, J.-M.; Chyan, C.-L.; Zhou, H.-X.; Chung, T.-Y.; Peng, H.; Ping, G.; Yang, G. *Protein Sci.* **2008**, in press.

(26) Talbot, J.; Jin, X.; Wang, N.-H. L. *Langmuir* **1994**, *10*, 1663.

(27) The area of lipid head groups is $\sim$60 Å^2. A membrane is a bilayer of lipids; hence, the area calculated on the basis of a single lipid molecule is $\sim$30 Å^2.

(28) In addition to the difference in shape for the cross section of the in-plane species, there are other subtle differences in the treatment of Aisenbrey et al. In dealing with the in-plane species's simultaneous presence in both leaflets, they left the chemical potential of the transmembrane as unaffected (corresponding to $\eta = 1$ in our model) but doubled the chemical potential of the in-plane species. The last step seems unjustified. Aisenbrey et al. also considered the influence of the surface charge brought by bound peptide according to the Gouy−Chapman theory; this influence is the same for the two peptide species and thus would not affect their equilibration.

(29) Po, M.-M.; Lam, J. W.; Orida, N.; Chao, A. W. *Biophys. J.* **1979**, *26*, 1.

(30) Note that the radius a of the membrane proteins is absorbed into the average area fraction $\langle\phi\rangle$.

(31) Bokvist, M.; Grobner, G. *J. Am. Chem. Soc.* **2007**, *129*, 14848.

(32) Fivaz, M.; Vilbois, F.; Thurnheer, S.; Pasquali, C.; Abrami, L.; Bickel, P. E.; Parton, R. G.; van der Goot, F. G. *EMBO J.* **2002**, *21*, 3989.

(33) Cunningham, O.; Andolfo, A.; Santovito, M. L.; Iuzzolino, L.; Blasi, F.; Sidenius, N. *EMBO J.* **2003**, *22*, 5994.

(34) Helms, J. B.; Zurzolo, C. *Traffic* **2004**, *5*, 247.

(35) Schreiber, G.; Haran, G.; Zhou, H.-X. *Chem. Rev.* **2009**, in press.

(36) Zhou, H.-X.; Szabo, A. *J. Chem. Phys.* **1991**, *95*, 5948.

(37) Szabo, A. *J. Phys. Chem.* **1989**, *93*, 6929.

(38) Knight, J. D.; Miranker, A. D. *J. Mol. Biol.* **2004**, *341*, 1175.

(39) Bokvist, M.; Lindstrom, F.; Watts, A.; Grobner, G. *J. Mol. Biol.* **2004**, *335*, 1039.

(40) Zhao, H.; Tuominen, E. K. J.; Kinnunen, P. K. J. *Biochemistry* **2004**, *43*, 10302.

(41) Jayasinghe, S. A.; Langen, R. *Biochemistry* **2005**, *44*, 12113.

(42) Apostolidou, M.; Jayasinghe, S. A.; Langen, R. *J. Biol. Chem.* **2008**, *283*, 17205.

(43) Heimburg, T.; Marsh, D. *Biophys. J.* **1995**, *68*, 536.

JP8107446